Langmuir

Article

pubs.acs.org/Langmuir

Modeling the Self-Assembly of Silica-Templated Nanoparticles in the Initial Stages of Zeolite Formation

Szu-Chia Chien,[†] Scott M. Auerbach,*[,‡] and Peter A. Monson*[,†]

[†]Department of Chemical Engineering and [‡]Department of Chemistry, University of Massachusetts, Amherst, Massachusetts 01002, United States

Supporting Information

ABSTRACT: The reaction ensemble Monte Carlo method was used to model the self-assembly and structure of silica nanoparticles found in the initial stages of the clear-solution synthesis of the silicalite-1 zeolite. Such nanoparticles, which comprise both silica and organic structure-directing agents (OSDAs), are believed to play a crucial role in the formation of silica nanoporous materials, yet very limited atomic-level structural information is available for these nanoparticles. We have modeled silica monomers as flexible tetrahedra with spring constants fitted in previous work to silica bulk moduli and OSDAs as spheres attracted to anionic silica monomers. We have studied one-step and two-step formation mechanisms, the latter involving the initial association of silica species and OSDAs driven by physical solution forces, followed by silica condensation/hydrolysis reactions simulated with reaction ensemble Monte Carlo. The two-step process with preassociation was found to be crucial for generating nearly spherical nanoparticles; otherwise, without preassociation they exhibited jagged, ramified structures. The two-step nanoparticles were found to exhibit a core−shell structure with mostly silica in the core surrounded by a diffuse shell of OSDAs, in agreement with SANS and SAXS data. The Q_n distribution, quantifying silicon atoms bound to n bridging oxygens, found in the simulated nanoparticles is in broad agreement with ^{29}Si solid-state NMR data on smaller, 2 nm nanoparticle populations. Ring-size distributions from the simulated nanoparticles show that five-membered rings are prevalent when considering OSDA/silica mole fractions (∼0.2) that lead to silicalite-1, in agreement with a previous IR and modeling study. Nanoparticles simulated with higher OSDA concentrations show ring-size distributions shifted to smaller rings, with three-membered silica rings dominating at an OSDA/silica mole fraction of 0.8. Our simulations show no evidence of long-range silicalite-1 order in these nanoparticles.

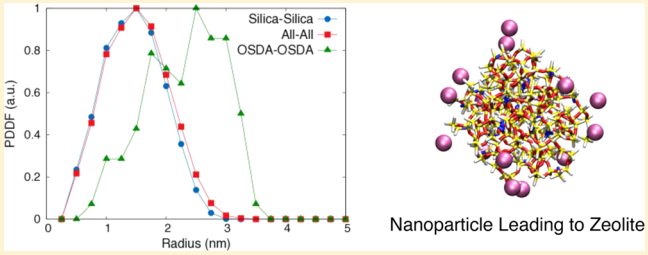

INTRODUCTION

Nanoporous materials are of great importance in chemical industries due to their wide application in many fields such as catalysis, separation, biotechnology, and microelectronics.[1−3] An ongoing theme in nanoporous materials research is the tailoring of pore structure and surface properties for specific applications.[4−7] Key to tailoring and controlling nanoporous materials is a better understanding of their formation mechanisms. To date, over 200 different zeolite structures have been fabricated (database of zeolite structures: http://www.iza-structure.org/databases/),[8] and several million more have been hypothesized.[9,10] However, because of limitations of characterization techniques in the critical 5−10 nm range of length scales, the understanding of their formation mechanisms remains largely incomplete.[5,11−14] Nanoparticles containing both silica and organic structure-directing agents (OSDAs) have been observed and implicated as important in the formation of all-silica zeolites.[13,15−20] Despite the importance of such nanoparticles, their atomic-level structures remain poorly understood because of the difficulty of isolating and characterizing such colloidal species. In this article, we apply reaction ensemble Monte Carlo to simulate a detailed molecular model of silica−OSDA self-assembly to reveal heretofore unknown structural properties of these nanoparticles.

The clear-solution synthesis provides an approach for fabricating silicalite-1 at relatively low silica concentrations, avoiding the complexities of silica gel formation. Experiments are usually carried out by adding tetraethylorthosilicate (TEOS) and a tetraalkylammonium (TAA) species—usually tetrapropylammounium (TPA)—as the OSDA to a basic aqueous solution to prepare silicalite-1.[13,21−23] TEOS initially undergoes hydrolysis to yield silicic acid monomers for silica polymerization. Such monomers subsequently undergo condensation and hydrolysis over time to yield the aforementioned silica−TAA nanoparticles. Small-angle X-ray scattering (SAXS) and small-angle neutron scattering (SANS) experiments have shown that the nanoparticles have a typical size of about 2−5 nm containing 250−400 Si atoms and a core−shell structure with a silica-rich core surrounded by an OSDA-rich

Received: January 29, 2015
Revised: April 7, 2015
Published: April 14, 2015

DOI: 10.1021/acs.langmuir.5b00382
Langmuir 2015, 31, 4940−4949

shell.[13,21,24,25] The core size of the obtained nanoparticles was found to decrease with pH, increase with temperature, and otherwise remain nearly independent of solution composition. No reproducible evidence of silicalite-1 structure has been observed in these silica−TAA nanoparticles.[24,25]

These nanoparticles are believed to transform into silicalite-1 crystals at long times and/or elevated temperatures,[13] thus possibly holding the key to understanding the formation mechanisms of silica zeolites. Several hypotheses have been proposed to explain the transformation of nanoparticles to silicalite-1 crystals. Schoeman et al. suggested that nanoparticles simply serve as sacrificial nutrients to feed the nucleation and growth of silicalite-1 crystallization,[11] and others have suggested a zeolite growth process via nanoparticle aggregation.[24−27] More recently, Lupulescu et al. have applied in situ atomic force microscopy (AFM) to study silicalite-1 growth.[28] The authors proposed a growth mechanism of silicalite-1, which is a combination of the direct attachment of nanoparticles and the nanoparticles acting as nutrients yielding smaller silica species that contribute to silicalite-1 formation. Tsapatsis and co-workers reported evidence for aggregative growth in a lengthy room-temperature study on 2−5 nm nanoparticles characterized by SAXS, atomic force microscopy (AFM), and transmission electron microscopy (TEM).[13] They observed after several hundred days of room-temperature aging the emergence of ∼10 nm aggregates with identifiable subdomains, clearly showing aggregation. These aggregates were subsequently found to provide nucleation centers for silicalite-1 nanocrystallites. Despite this progress, atomic-level structural information on these nanoparticles and their transformations has remained elusive.

In pursuit of such structural insights, Lesthaeghe et al. performed a combined quantum chemistry and infrared (IR) spectroscopy study on these nanoparticles, suggesting that these silica−TPA nanoparticles exhibit a modified version of the "pentasil" IR vibrational signature (∼550 cm^{-1}) observed from five-membered silica ring vibrations in silicalite-1.[26] They reported an IR peak for the nanoparticles that shifts from 650 cm^{-1} after 1 min of aging to ∼600 cm^{-1} after 46 min. Quantum chemistry calculations performed by these authors to interpret the IR data show that such blue shifts (from the signature ∼550 cm^{-1} feature) can arise from system size effects in the growing nanoparticles and from the details of the connectivity between various five-membered silica rings. Lesthaeghe et al. conclude that the synergistic combination of silica and TPA in these nanoparticles leads to a significant population of five-membered silica rings, a key building unit of the silicalite-1 structure. Their interpretation of the IR data warrants further study and exemplifies the difficulty with the direct experimental determination of nanoparticle structure.[6] Mora-Fonz et al. applied DFT with the COSMO approximation to solvation energy to study the chemistry of oligomerization processes of silica.[29,30] Detailed thermodynamic properties of the very initial stages of the silica polymerization process were obtained.

Several modeling techniques have been applied to investigate the formation mechanisms of nanoporous materials, with various levels of detail.[6,31] The requirements of modeling relatively long length and time scales and the interplay of physical and chemical interactions make this class of systems challenging to model. Rankin et al. introduced a dynamic Monte Carlo simulation to model silicic acid polymerization, which is a key reaction during the formation of zeolites.[32] Their method is based on solving material balances together with reaction rate expressions. This modeling approach has successfully reproduced the initial behavior of the Q_n distribution, where Q_n is the mole fraction of silicon atoms connected to n bridging oxygens. Because a given Q_n distribution does not uniquely specify the atomic-level structure, Wu and Deem developed an atomistic model to investigate the nucleation process of pure silica in the absence of OSDA species.[33]

They applied specialized Monte Carlo (MC) simulations to sample equilibrium structures of silica particles, suggesting that critical nuclei for pure silica crystallization may contain as few as 50 Si atoms but leaving the effects of OSDAs uncertain. Rao and Gelb studied early stages of silica polymerization using molecular dynamics (MD) simulation at high temperatures (1500−2500 K) over a wide range of silicic acid concentrations in water.[34] At high silicic acid concentration, monomers quickly react to form a large population of dimers, which later become depleted as larger clusters appear. At lower silicic acid concentrations, the polymerization is reaction-limited in the initial stages, which are dominated by the formation of dimers. They also estimated the activation energy of condensation to be 13−15 kcal/mol in excess water. In addition, continuum kinetic Monte Carlo simulations have been reported to model the very early stages of silica polymerization by van Santen and co-workers.[35−37] The silica condensation rate constants were computed using DFT and AIMD calculations. The model was further extended to study the silica oligomerization process by the lattice-gas kinetic Monte Carlo method. Their results suggest that the gelation process proceeds from four-membered rings, whereas five-membered rings and six-membered rings share Si with four-membered rings and form during the later gelation stages. Because of the computational demands of such atomistic modeling, these MC and MD methods could not approach the length and time scales needed to simulate the self-assembly of silica nanoparticles that lead to zeolites.

We have reported lattice model Monte Carlo simulations to describe the formation of silica−OSDA nanoparticles in the early stages of the clear-solution synthesis of silicalite-1.[38,39] Such models dramatically reduce the space of allowed configurations, allowing the study of much larger system sizes. Our studies reproduced the core−shell structure found in SAXS and SANS measurements and predicted the metastable nature of these nanoparticles found by Davis et al.[13] However, such lattice models cannot reveal the detailed structural information we seek herein.

To address this need, Malani et al. reported an off-lattice MC simulation of silica polymerization using the reaction ensemble MC method with specialized MC moves.[40,41] This approach has provided the best agreement to date with ^{29}Si NMR data on the evolution of the Q_n distribution[42] as well as atomic-level structural information on the evolution of ring-size distributions during the process of silica polymerization. The work of Malani et al. was restricted to the isoelectric point of silica (pH ∼2) and was conducted in the absence of OSDA. We now generalize these off-lattice reaction ensemble MC simulations to a wide range of pH values and in the presence of a simple model of an OSDA. We find below that reproducing known properties of these silica−OSDA nanoparticles such as size and shape requires a two-step process beginning with preassociation driven by physical solution forces, followed by silica polymerization with reaction ensemble MC. We also find that, when considering OSDA/silica mole fractions that lead to silicalite-1, the resulting simulated nanoparticles exhibit ring-size distribu-

DOI: 10.1021/acs.langmuir.5b00382
Langmuir 2015, 31, 4940−4949

tions dominated by five-membered silica rings, corroborating the work of Lesthaeghe et al.[26]

The remainder of this article is organized as follows: section 2 describes the model and simulation methodology; section 3 provides our nanoparticle structure; and section 4 offers a summary and concluding remarks.

MODEL AND SIMULATION METHODOLOGY

Molecular Model. This work makes use of a molecular model consisting of flexible, corner-sharing tetrahedra to represent silicic acid ($Si(OH)_4$) and silicate molecules ($Si(OH)_3O^-$) as neutral and anionic monomers for silica polymerization, respectively. (We do not consider species such as $[Si(OH)_2O_2]^{2-}$ in the present work because these are important only at very high pH, and we are interested here in more moderate alkaline conditions.) We also consider hard sphere particles with short-range attractions to represent OSDA molecules. The silica tetrahedron model was inspired by the "rigid unit mode" work of Dove[43] and was proposed in detail by Astala et al. for modeling the mechanical properties of crystalline silica solids.[44] OSDA molecules were taken to be spherical particles for simplicity; we will consider more complex OSDA structures in forthcoming work. Each silica tetrahedron is represented as a hard-sphere core in the center of each tetrahedron with four corners occupied by one of three possible oxygenic species: (i) hydroxyl groups (OH) represented as single particles, (ii) one oxide atom in the case of anionic silicate, and/or (iii) bridging oxygen atoms (BO) for condensed silica as shown in Figure 1a. The structure of each

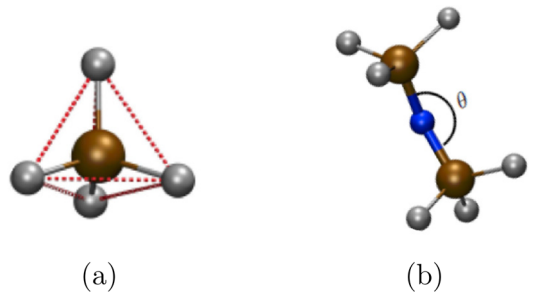

Figure 1. (a) Tetrahedral unit of silicic acid. A silicon atom (brown) is centered, and four hydroxyl groups (gray) are at the vertices. Dashed lines (red) connecting hydroxyl groups represent springs between them. (b) Silica dimer formed after a condensation reaction. Silicon atoms are connected through a bridging oxygen (blue) with a Si−O−Si angle (θ).[41]

flexible tetrahedron is maintained via harmonic springs between the various kinds of possible oxygen atoms according to

$$U_1 = \sum_{i=1}^{3}\sum_{j=i+1}^{4} \frac{k_S}{2}(|r_i - r_j| - r_0)^2 \quad (1)$$

where U_1 is the internal potential energy of a tetrahedron, r_i is the position of the ith BO/OH/O^- vertex, k_S is a spring constant, and r_0 is the equilibrium distance between two vertices (i.e., the oxygen−oxygen distance). The value of k_S was determined in previous work to be 851 kJ mol^{-1} $Å^{-2}$,[45] and r_0 is set at 2.61 Å on the basis of the geometry of silica tetrahedra (Si−O bond length = 1.6 Å and O−Si−O angle = 109.47°).[40,41]

In addition to specifying the energetics of each silica tetrahedron, it is also important to describe at a base-case level the energetics of the silica network. A general condensation/hydrolysis reaction taking place during silica polymerization can be written as

$$\equiv Si-OH + HO-Si\equiv \rightleftharpoons \equiv Si-O-Si\equiv + H_2O \quad (2)$$

where the forward reaction is condensation and the reverse reaction is hydrolysis. The polymerization process is thus viewed as the assembly of $Si(OH)_4$ and $Si(OH)_3O^-$ tetrahedra via condensation reactions. Two tetrahedra are connected via a bridging oxygen (Si−O−Si) after a condensation reaction occurs (as shown in Figure 1b). In our previous lattice model work on silica polymerization at high pH,[46] we have assumed for simplicity that such condensations occur only between terminal hydroxyls (OH) and not between OH/O^- or O^-/O^- groups; we will implement herein the application of this assumption to the present off-lattice model of silica polymerization. We have modeled the Si−O−Si angle formed by the bridging oxygen in our present work using the following harmonic potential

$$U_2 = \frac{k_A}{2}(\cos\theta - \cos\theta_0)^2 \quad (3)$$

where θ is the Si−O−Si angle formed by the bridging oxygen, θ_0 is a reference angle, and k_A is an angular force constant. The value of 155° was used for the reference Si−O−Si angle, and the value of 226.74 kJ mol^{-1} was used for k_A. Those values were determined by optimizing infinite silica chains using periodic DFT calculations[45] and were found to reproduce bulk moduli of silica polymorphs.[44] We note that the value of the reference angle falls roughly midway in the range of commonly observed Si−O−Si angles in silica materials (i.e., 130−180°).[47,48]

We have simulated nanoparticle formation as one-step and two-step processes. The one-step process goes directly into reaction ensemble Monte Carlo to simulate polymerization. In contrast, the two-step procedure begins with a preassociation step to form silica−OSDA clusters that are held together by physical solution forces. Silica polymerization is then allowed to take place to condense the clusters into silica networks. The rationale behind the two-step approach comes from previous nonreactive simulations of Catlow and co-workers,[49] which found that silica species tend to cluster in aqueous solutions, even under dilute conditions, perhaps driven by a measure of hydrophobicity. The two-step process described above is also reminiscent of the two-step procedure for synthesizing silica mesoporous solids such as MCM-41,[46] involving an initial step to produce silica−surfactant mesoscale order, followed by silica network condensation at elevated temperatures.

To model the preassociation of silicic acids, we applied the Stillinger−Weber (SW) potential for the interaction between neutral and anionic silica monomers. This potential, which comprises two-body and three-body interactions, was first proposed to model solid and liquid forms of silicon.[50] The SW model has also been applied to water molecules, carbon, and germanium—all tetrahedrally coordinated units.[51] We apply SW herein as a smooth potential that mimics the anharmonicity of a square well because such anharmonicity provides liquidlike flexibility that is important for facilitating subsequent silica polymerization.

In the SW potential, tetrahedral coordination is enforced by the three-body term. However, as introduced previously, our model already includes harmonic interactions (eq 3) to restrict Si−O−Si angles. In addition, calculating three-body potentials can become computationally intensive. As such, we apply in this work only the two-body SW potential given by

DOI: 10.1021/acs.langmuir.5b00382
Langmuir 2015, 31, 4940−4949

$$\varphi_2(r) = A\epsilon\left[B\left(\frac{\sigma}{r}\right)^p - \left(\frac{\sigma}{r}\right)^q\right]\exp\left(\frac{\sigma}{r - a\sigma}\right) \quad (4)$$

where A is 7.05, B is 0.602, p is 4, q is 0, and reduced cutoff a is 1.8 to ensure the potential and forces go to zero at a distance of $a\sigma$. These are the standard parameters of the Stillinger−Weber potential.[50]

The SW potential well depth, ϵ, was taken to be 6.0 and 12.0 kJ/mol for the neutral−neutral and anionic−neutral silica interactions, respectively. These well depths were chosen to be less than the energy scale of silica polymerization so that in the second stage of the simulation, where such polymerization takes place, our results will yield substantial and experimentally reasonable degrees of condensation. This model uses 4.5 Å for σ; the value has been shown to lead to a first shell at about 5 Å in the radial distribution function of the silica solution, which is consistent with the one calculated by Pereira et al.[49] Note that there is no SW interaction between two chemically bound silica tetrahedra (i.e., two silica tetrahedra that are connected through a bridging oxygen).

In addition to the interaction between silica tetrahedra, an attraction between charged species—anionic silica and cationic OSDA—is also included. As a substantial amount of screening between charged species is expected in the solution phase, and the electrostatic potential is modeled using short-range attractions with the simplified SW potential (i.e., only the two-body potential). This short-range interaction enforces local charge balancing, which likely plays a role in inorganic material growth. The same value of σ in the silica pairwise interaction was applied to the SW potential binding anionic silica and cationic OSDA, whereas the larger well depth of 36 kJ/mol was applied to describe the charge-balancing interaction between anionic silica and cationic OSDA. Previous MD simulations by Vlachos and co-workers[52] find that a free-energy well depth for silicate−TMA interactions is on the order of 20 kJ/mol. We apply a slightly larger well depth in our present simulations, 36 kJ/mol, which we find is necessary in the context of the present coarse-grained model to produce nanoparticles associated with OSDA species.

Various Stillinger−Weber potential wells for the neutral−anionic silica interaction and the $OSDA^+$−anionic silica interaction were tested in our simulations. With more favorable interactions between neutral and anionic silica (i.e., from 6 to 10 kJ/mol), the silica cluster size was found to increase. The cluster size, however, remains nearly constant when the neutral−anionic silica interaction is greater than 11 kJ/mol. Varying the $OSDA^+$−anionic silica interactions from 25 to 75 kJ/mol was found to leave the nanoparticles size essentially unchanged.

Sampling and Methodologies. Each simulation started with a random configuration in a cubic box with dimensions of 192 Å × 192 Å × 192 Å, giving sufficient volume to simulate the early stages of clear-solution zeolite synthesis. Specifically, it needs to be large enough to accommodate several nanoparticles without their agglomerating to form a gel as occurred in our previous low-pH studies.[40,41] For both one-step and two-step processes, we studied compositions given by TEOS/OSDA = 1000:x including 1000 TEOS molecules and x = 0, 100, 200, 300, 400, 500, 600, 700, 800, or 900 OSDA molecules. In general, we focus below on results from the TEOS/OSDA = 1000:200 composition because this most closely resembles typical clear-solution zeolite synthesis conditions.[21,22] We assumed that TEOS hydrolysis is rapid compared to all other processes, yielding 1000 silicic acid molecules randomly placed in the simulation box at the beginning of the simulation. We also assumed that cationic OSDA is introduced as its hydroxide salt $[OSDA^+(OH^-)]$, producing an equal number of anionic silicate monomers and cationic OSDA molecules, assuming completion of the strong base (OH^-)/weak acid $(Si(OH)_4)$ reaction. As such, each simulation began with x OSDA species, x anionic silicate monomers, and 1000 − x silicic acid monomers, all initially placed randomly in the simulation cell.

In each simulation, at least 2 million MC steps were performed to allow sufficiently complete structural assemblies. The MC moves included random translations performed on all species, including anionic−silicate−$OSDA^+$ pairs, and rotations performed on all silica tetrahedron (i.e., nonspherical species) in the canonical (NVT) ensemble to sample all possible spatial configurations. Furthermore, to sample reaction events in our simulations, the reaction ensemble MC (REMC) technique[53,54] was used to simulate silica polymerization. REMC provides a convenient way to study self-assembly arising from silica polymerization at ambient temperature. REMC also eliminates the need for reactive force fields to bring about the assembly of the polymerized silica network. Our choice for the REMC technique is further supported by the recent simulation study of Malani et al., where they studied silica polymerization at a low pH value (∼2) corresponding to the isoelectric point of silica.[40,41] REMC was performed on the two OH groups within a distance of only 2 Å to mimic the real behavior of the condensation reaction. In general, our attempt probabilities for moves were chosen to be 0.79 for translations on all species, 0.20 for tetrahedron rotations, and 0.01 for REMC moves.

In the REMC method, the probability for accepting reactive moves is given by

$$P_{\text{rxn}} = e^{-\beta\Delta U}V^{\bar{\nu}}\prod_{i=1}^{n_c}\frac{N_i!}{(N_i+\nu_i)!}q_i^{\nu_i} = e^{-\beta\Delta U}V^{\bar{\nu}}K_{\text{eq}}\prod_{i=1}^{n_c}\frac{N_i!}{(N_i+\nu_i)!} \quad (5)$$

where ΔU is the change in potential energy arising from tetrahedral and network distortions, V is the volume, n_c is the total number of components, $\bar{\nu} = \sum_{i=1}^{n_c}\nu_i$, and q_i, N_i, and ν_i are the molecular partition function, number of molecules, and stoichiometric coefficient of component i, respectively. The molecular partition functions q_i are related to the equilibrium constant and standard Gibbs free energy of reaction via $K_{\text{eq}} = e^{-\Delta G_0/k_BT} = \prod_{i=1}^{n_c}q_i^{\nu_i}$. We simplify the calculations by using the standard Gibbs energy of reaction as an input parameter in the calculation. In our study, all reaction types are assumed for simplicity to have the same value of the standard Gibbs free energy. We have used K_{eq} = 500 in this work and in our previous studies, corresponding to a condensation free energy at T = 300 K of −15.5 kJ/mol = −3.7 kcal/mol. This number, 500, is in reasonable agreement with the electronic energy change of −3.2 kcal/mol obtained from a DFT calculation on silicic acid dimerization in water.[55] More detailed information on our simulation methods and MC sampling moves can be found in the previously published papers from our group.[40,41] As described above, we considered one-step (polymerization) and two-step (preassociation followed by polymerization) silica self-assembly processes. In the two-step process, we generally carried out 2 million preassociation MC steps (translations and rotations), followed by 2 million polymerization steps (translations, rotations, and REMC steps).

DOI: 10.1021/acs.langmuir.5b00382
Langmuir 2015, 31, 4940−4949

RESULTS AND DISCUSSION

In this section, we discuss the simulation results on the formation and structural characteristics of the silica−OSDA nanoparticles. We begin by briefly discussing the one-step process, followed by a more thorough description of results for the two-step process.

One-Step Process. We begin by discussing the one-step simulation with the TEOS/OSDA = 1000:200 composition system. This simulation proceeds directly to silica polymerization from a random initial condition without any preassociation. Figure 2 shows that this produces relatively

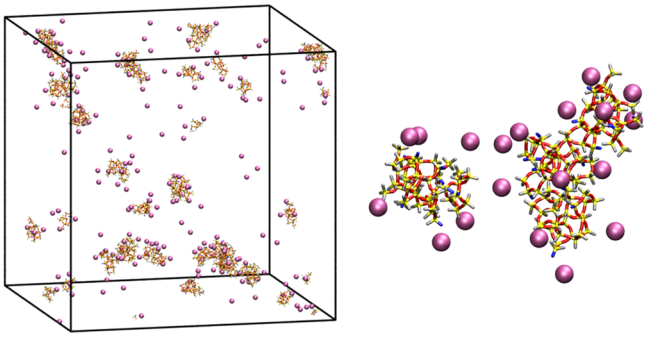

Figure 2. Ramified, highly nonspherical, and relatively small clusters of silica and OSDA obtained from the one-step formation process. Color code: Si (yellow), oxide (blue), bridging oxygen (red), hydroxyl (gray), and OSDA (purple).

small nanoparticles with highly nonspherical shapes, in contrast to the roughly spherical particles observed from experiments.[21] In particular, the one-step simulations produce nanoparticles with diameters consistently less than 1.5 nm and with ∼20 Si tetrahedra, in comparison to the 2−5 nm nanoparticles found in experiments containing several hundred Si tetrahedra.[13] This result suggests that silica polymerization in the earliest stages of nanoparticle formation may substantially suppress further nanoparticle growth, presumably because the hydrolysis of Si−O−Si linkages releases too few silica tetrahedra for mass transport among nanoparticles. This finding also suggests that nonreactive silica preassociation may be important for nanoparticle formation,[49] which we discuss in the next section.

To track silica polymerization during the one-step process, the Q_n distribution was computed as the reaction proceeded. The evolution of the Q_n distribution for the TEOS/OSDA = 1000:200 system is shown in Figure 3. It can be seen that Q_0 and Q_1 cross at a mole fraction of ∼0.4, whereas the mole fraction at the Q_0/Q_2 crossing is around 0.2 and that for Q_0/Q_3 is around 0.1. In principle, the pattern of crossing points and maxima in the Q_n distribution provides a signature describing the polymerization process; we find that the evolution of the Q_n distribution for silica gel formation simulated previously by Malani et al.,[41] the one-step nanoparticle formation shown in Figure 3, and the two-step nanoparticle formation (Figure S1 in Supporting Information) show substantially similar patterns suggesting similar polymerization mechanisms. One difference pertains to the overall degree of polymerization, which is given by

$$c = \left(\frac{1}{f}\right)\Sigma_{n=0}^{f}\, nq_n \qquad (6)$$

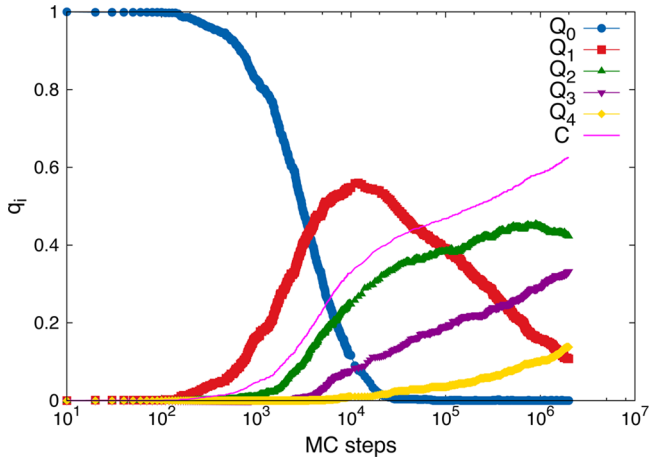

Figure 3. Evolution of the Q_n distribution during polymerization obtained from the one-step formation process.

where q_n is the mole fraction of Q_n silicon atoms and f is the coordination number of the network (normally f = 4 in this case).

In our previous simulations of gel formation,[41] the degree of polymerization was found to reach a value of around 0.8 after 10^5 MC steps, indicating that 80% of the terminal oxygens transformed into bridging oxygens. Figure 3 shows a final degree of polymerization of around 0.6 after 2 million MC steps; a similar degree of polymerization was found for the two-step process applied to the TEOS/OSDA = 1000:200 system. This decrease of 0.2 in the degree of polymerization is consistent with 20% of the silica tetrahedra being anionic silicate with a maximum allowed coordination number of 3. This finding may explain why we see so little Q_4 silica in our nanoparticles, with Q_4 mole fractions reaching values that are little more than 0.1, whereas in the gel we found Q_4 mole fractions of 0.3. We compare Q_n mole fractions to experiment in the next section on the two-step process, finding good overall agreement with NMR data.

Two-Step Process. Here we show results for the two-step process involving nonreactive preassociation MC driven by the SW potential, followed by silica polymerization simulated with REMC. The resulting nanoparticles were found to exhibit a core−shell structure with most of the silica in the core and OSDA molecules at the surface of the nanoparticles, as shown in Figure 4.

Such core−shell structure was observed experimentally via SAXS and SANS characterization techniques.[21,22] Pair−distance distribution functions (PDDFs) can be extracted from the SAXS and SANS data. PDDFs from SAXS are more sensitive to the relatively high electron density of the silicon atoms in the silica core, whereas PDDFs from SANS tend to reveal the structure of the entire nanoparticle, receiving signals from both lighter and heavier elements. For comparison with PDDFs from SAXS and SANS, we have computed PDDFs among silica tetrahedra and among all particles, respectively. We have also computed PDDFs among OSDA molecules; all of these and the experimental results[21] are shown in Figure 5. The silica−silica PDDF has a peak at around 1.5 nm, indicating a particle core size of around 3.0 nm, in good agreement with experiments which find silica−OSDA nanoparticles in the 2−5 nm range.[13,21,22] The all−all PDDF in Figure 5 is essentially the same as the silica−silica PDDF because the number of silica tetrahedra significantly exceeds that of the OSDAs, making the

DOI: 10.1021/acs.langmuir.5b00382
Langmuir 2015, 31, 4940−4949

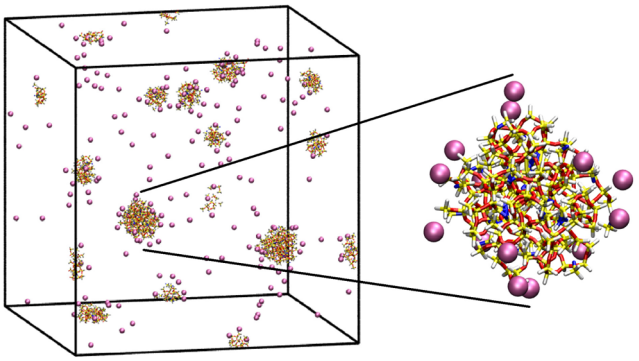

Figure 4. Snapshots of nanoparticles obtained from the two-step formation process in the system with TEOS/OSDA = 1000:200. Color code: Si (yellow), oxide (blue), bridging oxygen (red), hydroxyl (gray), and OSDA (purple).

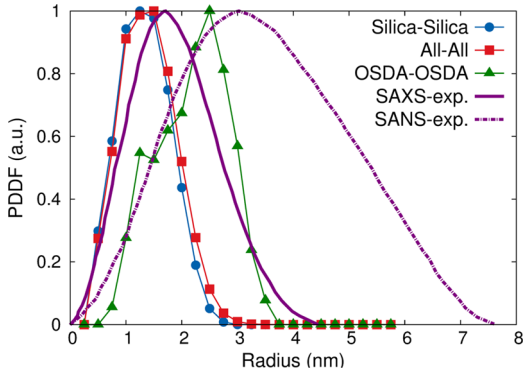

Figure 5. Core–shell structure shown by pair–distance distribution functions (PDDFs) among silica tetrahedra, all particles, and OSDAs; from simulations with composition TEOS/OSDA = 1000:200; and experimental PDDFs of SAXS and SANS patterns of a nanoparticle solution (40:9:9500:320 SiO_2/TPAOH/H_2O/TEOS) from the literature.[21]

statistical effect of the OSDAs minimal in the all–all graph. This is a consequence of the coarse graining of the OSDA from 41 atoms, in the case of TPA, to 1 lumped particle. The simulated OSDA–OSDA PDDF reveals that OSDAs exist in a shell about 1 nm larger than the silica core, which makes sense given that the 4.5 Å Stillinger–Weber length scale is multiplied by 2 because distal OSDAs are on opposite sides of a given nanoparticle. In contrast, PDDFs from experimental SAXS and SANS data reveal a 3.5 nm difference between the silica core and TPA shell, which likely arises from the details of Debye screening in solution not accounted for by our model. In future work, we will consider more complex models of OSDA structure and OSDA–silicate interactions to build on the insights gained from the base case model presented herein.

Detailed visualizations of nanoparticles from a single simulation with a range of sizes are shown in Figure 6a. The numbers of OSDAs at the surfaces of these nanoparticles are 15, 12, and 9 for nanoparticles composed of 208, 148, and 108 silica tetrahedra, respectively, corresponding to a mean OSDA/silica ratio of 0.09, well in excess of the ratio in as-made TPA–silicalite of 4:92 TPA/SiO_2 per unit cell. The PDDFs for distances among silica tetrahedra for these particles are shown in Figure 6b. These PDDFs reveal that these particles have sizes ranging roughly from 2 to 3.5 nm, in good agreement with experimental observations.[21,22] In addition, the densities of the

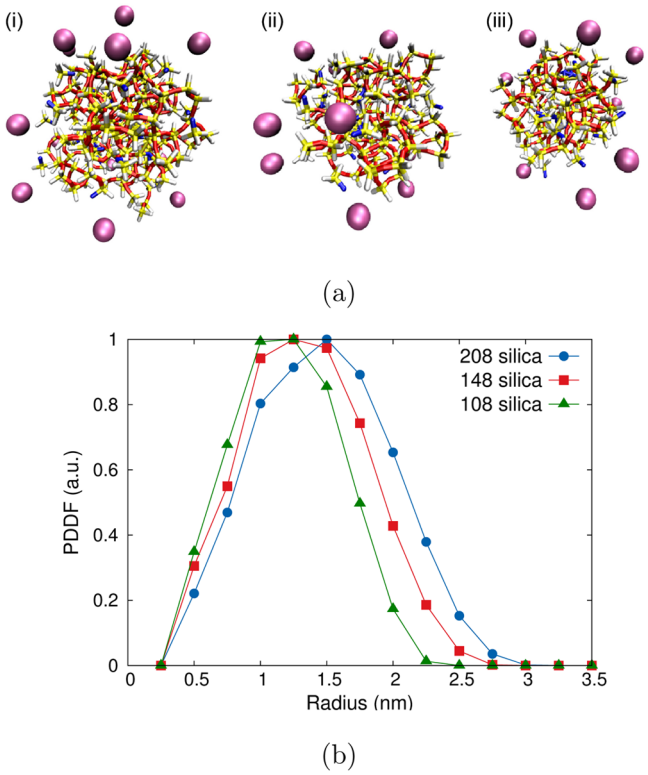

Figure 6. (a) Snapshots of nanoparticles with the number of silica tetrahedra being (i) 208, (ii) 148, and (iii) 108. Color code: Si (yellow), oxide (blue), bridging oxygen (red), hydroxyl (gray), and OSDA (purple). (b) PDDFs (silica–silica) of nanoparticles corresponding to the snapshots.

simulated nanoparticles shown in Figure 6a were calculated from the number of atoms and the particle sizes extracted from PDDFs. It was found that the density is in the range of 1.68–1.83 g/cm^3, which is in good agreement with the experimental value of 1.75 g/cm^3 reported by Rimer et al.[56]

Now we consider the effect of varying the initial composition according to TEOS/OSDA = 1000:x, where x varies as 0, 100, 200, ..., 900. We have found that the number of OSDA molecules has a substantial effect on the topology of the resulting nanoparticles. For example, Figure 7 shows a simulated nanoparticle (front and side views) from a simulation with composition TEOS/OSDA = 1000:500 (on the left-hand side) and TEOS/OSDA = 1000:800 (on the right-hand side), showing an ordered arrangement of neutral silicate and anionic silicate. We note that only a few bridging oxygens form in the

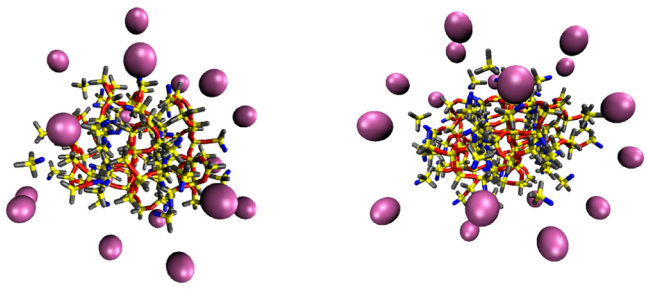

Figure 7. Snapshot of particles with an ordered arrangement of neutral silica and anionic silica. Color code: Si (yellow), oxide (blue), bridging oxygen (red), hydroxyl (gray), and OSDA (purple).

DOI: 10.1021/acs.langmuir.5b00382
Langmuir 2015, 31, 4940–4949

particles. However, such an ordered arrangement of nanoparticles was found to exhibit lower degrees of polymerization and hence may be too unstable to survive in experiments at longer observation times.

We have found that the number of OSDA molecules plays an important role in determining the sizes of clusters in the preassociation step. Figure 8 shows the average maximum

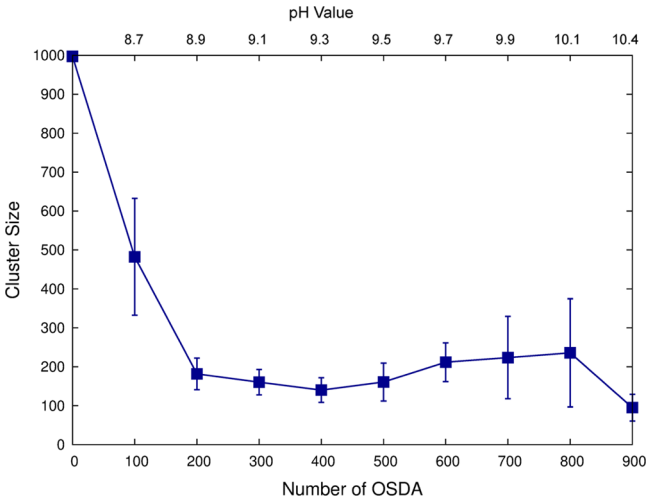

Figure 8. Maximal cluster size obtained from the preassociation process after performing 2 million MC steps.

cluster size as a function of the number of OSDA molecules obtained from 20 independent simulations. When considering no OSDA, the system evolves to a single cluster consisting of almost all available silicic acids. With the addition of 100 OSDA molecules to the system, the interplay between OSDA and silica leads to smaller clusters. Considering systems with ≥200 OSDA molecules produces cluster sizes that are roughly constant with respect to the number of OSDAs. We have also observed in our simulations that as the silica preassociation process proceeds, the dissolution of smaller clusters contributes to the growth of larger clusters, following Ostwald ripening.[38] We have also extracted OSDA surface coverages by defining an OSDA−Si distance criterion corresponding to half the Stillinger−Weber well depth. After analysis, we found that OSDA surface coatings depend on the number of OSDAs in the simulation and on the nanoparticle size, as shown in Figure S2 in Supporting Information. Surface coverages were obtained for TEOS/OSDA = 1000:x, where x = 100−900. We have found a plateau effect for x > 300 and a log(OSDA) − log(Si) slope of 0.61 ± 0.15, indicating a surface coverage scaling (expected exponent of $^2/_3$). In the plateau range, the mole fractions for small clusters are around 1:4 OSDA/Si, whereas those for large clusters are around 1:12 OSDA/Si. For comparison, silicalite-1 with TPA at each intersection corresponds to 1:24, indicating by this standard that these nanoparticles are generally rich in OSDA.

Table 1 shows the Q_n distribution of the final configuration of nanoparticles simulated for TEOS/OSDA = 1000:200, compared to several experimental Q_n distributions. The experimental data in Table 1 include Q_n distributions from two studies on 3−5 nm nanoparticles[57,58] and from a study on smaller, 2 nm nanoparticles.[27] The simulated Q_n distribution was computed from nanoparticles consisting of more than 100 silica tetrahedra to eliminate spurious statistics from small

Table 1. Comparison of Q_n Distributions for Silica−OSDA Nanoparticle Populations of Various Sizes Obtained from Our Simulation and from Experiments

mole fraction of Q_n silicon	Q_0	Q_1	Q_2	Q_3	Q_4
our simulation	0	12.9	35.2	37.8	14.1
experiment a (2 nm)[27]	0	<10	40−50	40−50	0
experiment b (3−5 nm)[57]	0	0	8.3	40.6	51.1
experiment c (3−5 nm)[58]	0	0	6.4	43.5	50.1

clusters. Table 1 indicates that the simulated Q_n distribution is in much better agreement with experimental data on the 2 nm nanoparticle population, showing high Q_2 and Q_3 fractions and low Q_4 fractions. Larger nanoparticles, especially aggregates of smaller nanoparticles, have been hypothesized to lead to silicalite-1 crystallization.[13] This is consistent with the notion that larger nanoparticles should exhibit higher Q_4 fractions, considering that crystalline silica consists almost exclusively of Q_4 silicon species. The nanoparticles formed during our simulations are in the smaller range of 2−3.5 nm, and condensation processes have not yet plateaued by the end of our simulations as evidenced by the nonzero slope in the degree of polymerization (Figure 3), suggesting that the population of nanoparticles that self-assemble in our simulations represents the nascent nanoparticles isolated by Aerts et al.[27] Despite the advances in model development and Monte Carlo simulation reported in this work, it remains computationally challenging to simulate the self-assembly of larger (>4 nm) silica−OSDA nanoparticles.

Our simulations allow a detailed structural analysis of early-stage precursor nanoparticles. The simulated nanoparticles exhibit no discernible short- or medium-range order. In the absence of such order, we focus on ring-size distributions as a structural descriptor of disordered silica. Figure 9 shows the

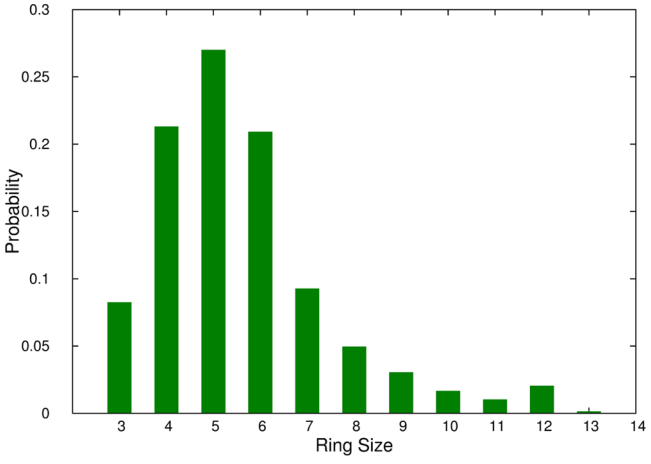

Figure 9. Computed ring-size distribution from the TEOS/OSDA = 1000:200 system.

computed ring-size distribution for the TEOS/OSDA = 1000:200 system using an algorithm that counts primitive rings in disordered networks.[59] These results were obtained by averaging ring-size distributions from nanoparticles with more than 100 silica tetrahedra, consistent with the Q_n analysis above. The ring-size distribution in Figure 9 is slightly different from that of silica gels, which was shown by Malani et al.[41] to be dominated by four-membered rings (involving four alternating, adjacent silicon and oxygen atoms). In contrast, the ring-size

DOI: 10.1021/acs.langmuir.5b00382
Langmuir 2015, 31, 4940−4949

distribution in Figure 9 exhibits a plurality of five-membered rings, a key component of the silicalite-1 framework structure.[8] A detailed investigation of the simulated nanoparticles shows no evidence of the presence of pentasil units, higher-order building units of the silicalite-1 structure involving chains of five-membered rings.[8] As such, our simulations predict that the atomic structures of these nanoparticles show no evidence of MFI structure other than the predominance of five-membered silica rings. Our results nonetheless support the experiments and quantum chemistry calculations of Lesthaeghe et al.,[26] who report IR spectroscopy evidence for the importance of five-membered rings in silica−OSDA precursor nanoparticles.

We also calculated the radius of gyration of each nanoparticle, the center-of-mass of all four-membered rings and five-membered rings, and the distance distribution of each of these rings relative to the center-of-mass of a given nanoparticle for the system of TEOS/OSDA = 1000:200. The relative position of rings in the nanoparticles is defined as

$$\text{relative position} = \frac{D_{\text{rings}}}{R_{\text{g}}} \tag{7}$$

where D_{rings} is the distance of the center-of-mass of a given four-membered ring or five-membred ring to the center of mass of a given nanoparticle and R_{g} is the radius of gyration of the corresponding nanoparticle. A histogram of the probability of the relative position is shown in Supporting Information as Figure S3. Figure S3 shows that five-membered rings are closer to the surface of nanoparticles than are four-membered rings.

Computed ring-size distributions for systems with various TEOS/OSDA ratios are shown in Figure 10. For the

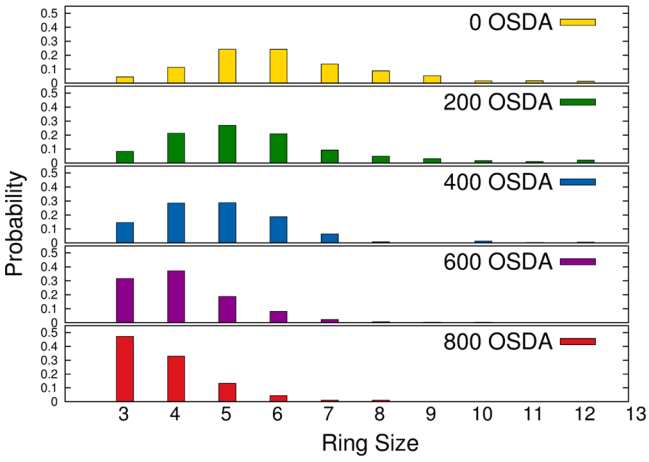

Figure 10. Ring-size distributions as a function of OSDA content.

simulations without OSDA there is a roughly equal population of five- and six-membered rings, in contrast to the situation in the simulated gel,[41] which is dominated by four-membered rings. Simulations with 200 and 400 OSDA molecules show a plurality of five-membered rings, whereas 600 and 800 OSDA molecules are dominated by four-membered rings and three-membered rings, respectively. The trend predicted in our simulations of the predominance of smaller rings arising from higher OSDA content is interesting and worthy of experimental testing, perhaps with Raman spectroscopy, which is a powerful tool for probing collective vibrations in silica networks.[60] It is also important to consider more accurate representations of OSDAs such as TPA to determine the extent to which the predicted trend in Figure 10 is influenced by the assumed representation of OSDAs. These results predict that the silica/OSDA composition may not only influence nanoparticle shape but also impact ring formation in the early stages of precursor nanoparticle self-assembly. It is interesting to consider whether the rings formed during these early stages may be important in determining which zeolites crystallize from a sample of precursor nanoparticles.

CONCLUSIONS

We have applied the reaction ensemble Monte Carlo method to sample an off-lattice model of silica association and polymerization to investigate structures of nanoparticles formed from silica and organic structure-directing agents (OSDAs) used for zeolite fabrication. We are particularly interested in modeling silica−OSDA nanoparticles that have been studied extensively when using tetrapropyl ammonium (TPA) as the OSDA in the clear-solution synthesis of silicalite-1. We have applied a previously developed model of silica monomers as flexible tetrahedra with spring constants fitted in previous work to reproduce the mechanical properties of silica. OSDAs were modeled in the present work as spheres attracted to anionic silica monomers. We have studied nanoparticle self-assembly by comparing one-step and two-step formation mechanisms. The one-step process goes directly into sampling silica polymerization via reaction ensemble Monte Carlo, whereas the two-step process begins with the nonreactive preassociation of silica species and OSDAs driven by physical solution forces, followed by silica polymerization simulated with reaction ensemble Monte Carlo. We have characterized the resulting nanoparticles using the particle size, shape, pair−distance distribution functions, Q_n distributions, and ring-size distributions.

The two-step process with preassociation was found to be crucial for generating sufficiently large and nearly spherical nanoparticles; otherwise, without preassociation the resulting nanoparticles were found to be rather small (>100 silica tetrahedra) and to have jagged, ramified structures. The two-step nanoparticles exhibit a core−shell structure, with mostly silica in a core of size 2−4 nm, surrounded by a diffuse shell of OSDAs with a thickness of about 1 nm, in broad agreement with SANS and SAXS data. The computed Q_n distribution, quantifying silicon atoms bound to n bridging oxygens, is in good agreement with ^{29}Si solid-state NMR data on smaller, 2 nm nanoparticles. Ring-size distributions from the simulated nanoparticles for systems with TEOS/OSDA = 1000:200 (i.e., for compositions that lead to silicalite-1) show that five-membered rings are prevalent, in agreement with a previous IR and quantum chemistry study. Nanoparticles simulated with higher OSDA concentrations show ring-size distributions shifted to four-membered silica rings. Our simulations show no evidence of medium-range silicalite-1 order in these nanoparticles, such as the presence of pentasil chains.

Our simulations include relatively simple, base-case representations of the OSDA and its interaction with silica, approximations that are crucial to our computational ability to simulate the self-assembly of nanoparticles on the 2−3.5 nm length scale. These initial approximations leave great scope for further refinements to the model, allowing future investigation into the role of OSDA molecular structure in nanoparticle formation and network structure and the role of longer-ranged OSDA−silica interactions in the nature of the core−shell structure in these nanoparticles. In particular, in forthcoming work we will study how more accurate molecular representa-

DOI: 10.1021/acs.langmuir.5b00382
Langmuir 2015, 31, 4940−4949

tions of OSDAs such as TPA influence ring-size distributions in silica−OSDA nanoparticles. Despite the simplicity of the present model, this work represents the first atomic-level model of the self-assembly of precursor silica−OSDA nanoparticles, opening the door to unprecedented insights into the formation of ordered nanoporous materials.

■ ASSOCIATED CONTENT

Supporting Information

Evolution of the Q_n distribution during polymerization obtained from the two-step formation process with TEOS/OSDA = 1000:200. Surface coverage of OSDA on the obtained silica clusters for TEOS/OSDA = 1000:*x*. Relative position of four-membered rings and five-membered rings in the obtained nanoparticles with TEOS/OSDA = 1000:200. This material is available free of charge via the Internet at http://pubs.acs.org.

■ AUTHOR INFORMATION

Corresponding Authors

*E-mail: auerbach@chem.umass.edu.
*E-mail: monson@ecs.umass.edu.

Notes

The authors declare no competing financial interest.

■ ACKNOWLEDGMENTS

This work was supported by a grant from the U.S. Department of Energy (contract no. DE-FG02-07ER46466). This research acknowledges the computational resources provided by the Massachusetts Green High-Performance Computing Center (MGHPCC).

■ REFERENCES

(1) Coronas, J. Present and future synthesis challenges for zeolites. *Chem. Eng. J.* **2010**, *156*, 236−242.
(2) Tang, F.; Li, L.; Chen, D. Mesoporous silica nanoparticles: synthesis, biocompatibility and drug delivery. *Adv. Mater.* **2012**, *24*, 1504−1534.
(3) Na, K.; Choi, M.; Ryoo, R. Recent advances in the synthesis of hierarchically nanoporous zeolites. *Microporous Mesoporous Mater.* **2013**, *166*, 3−19.
(4) Corma, A. From microporous to mesoporous molecular sieve materials and their use in catalysis. *Chem. Rev.* **1997**, *97*, 2373−2420.
(5) Auerbach, S. M., Carrado, K. A., Dutta, P. K. *Handbook of Zeolite Science and Technology*; Marcel Dekker: New York, 2003.
(6) Auerbach, S. M.; Ford, M. H.; Monson, P. New insights into zeolite formation from molecular modeling. *Curr. Opin. Colloid Interface Sci.* **2005**, *10*, 220−225.
(7) Barton, T. J.; Bull, L. M.; Klemperer, W. G.; Loy, D. A.; McEnaney, B.; Misono, M.; Monson, P. A.; Pez, G.; Scherer, G. W.; Vartuli, J. C.; Yaghi, O. M. Tailored porous materials. *Chem. Mater.* **1999**, *11*, 2633−2656.
(8) Baerlocher, C.; McCusker, L. B.; Olson, D. H. *Atlas of Zeolite Framework Types*, 6th ed.; Elsevier, 2007.
(9) Earl, D. J.; Deem, M. W. Toward a database of hypothetical zeolite structures. *Ind. Eng. Chem. Res.* **2006**, *45*, 5449−5454.
(10) Deem, M. W.; Pophale, R.; Cheeseman, P. A.; Earl, D. J. Computational discovery of new zeolite-like materials. *J. Phys. Chem. C* **2009**, *113*, 21353−21360.
(11) Schoeman, B. J. Analysis of the nucleation and growth of TPA-silicalite-1 at elevated temperatures with the emphasis on colloidal stability. *Microporous Mesoporous Mater.* **1998**, *22*, 9−22.
(12) Houssin, C. J. Y.; Kirschhock, C. E. A.; Magusin, P. C. M. M.; Mojet, B. L.; Grobet, P. J.; Jacobs, P. A.; Martens, J. A.; van Santen, R. A. Combined in situ ^{29}Si NMR and small-angle X-ray scattering study of precursors in MFI zeolite formation from silicic acid in TPAOH solutions. *Phys. Chem. Chem. Phys.* **2003**, *5*, 3518−3524.
(13) Davis, T. M.; Drews, T. O.; Ramanan, H.; He, C.; Dong, J.; Schnablegger, H.; Katsoulakis, M. A.; Kokkoli, E.; McCormick, A. V.; Penn, R. L.; Tsapatsis, M. Mechanistic principles of nanoparticle evolution to zeolite crystals. *Nat. Mater.* **2006**, *5*, 400−408.
(14) Rimer, J. D.; Trofymluk, O.; Lobo, R. F.; Navrotsky, A.; Vlachos, D. G. Thermodynamics of silica nanoparticle self-assembly in basic solutions of monovalent cations. *J. Phys. Chem. C* **2008**, *112*, 14754−14761.
(15) Burkett, S. L.; Davis, M. E. Mechanisms of structure direction in the synthesis of pure-silica zeolites. 1. Synthesis of TPA/Si-ZSM-5. *Chem. Mater.* **1995**, *7*, 920−928.
(16) Kirschhock, C. E. A.; Ravishankar, R.; Verspeurt, F.; Grobet, P. J.; Jacobs, P. A.; Martens, J. A. Identification of precursor species in the formation of MFI zeolite in the TPAOH-TEOS-H_2O system. *J. Phys. Chem. B* **1999**, *103*, 4965−4971.
(17) de Moor, P.-P. E. A.; Beelen, T. P. M.; Komanschek, B. U.; Beck, L. W.; Wagner, P.; Davis, M. E.; van Santen, R. A. Imaging the assembly process of the organic-mediated synthesis of a zeolite. *Chem.—Eur. J.* **1999**, *5*, 2083−2088.
(18) Bonilla, G.; Diaz, I.; Tsapatsis, M.; Jeong, H.-K.; Lee, Y.; Vlachos, D. G. Zeolite (MFI) crystal morphology control using organic structure-directing agents. *Chem. Mater.* **2004**, *16*, 5697−5705.
(19) Moliner, M.; Rey, F.; Corma, A. Towards the rational design of efficient organic structure-directing agents for zeolite synthesis. *Angew. Chem., Int. Ed.* **2013**, *52*, 13880−13889.
(20) Moteki, T.; Keoh, S. H.; Okubo, T. Synthesis of zeolites using highly amphiphilic cations as organic structure-directing agents by hydrothermal treatment of a dense silicate gel. *Chem. Commun.* **2014**, *50*, 1330−1333.
(21) Fedeyko, J. M.; Rimer, J. D.; Lobo, R. F.; Vlachos, D. G. Spontaneous formation of silica nanoparticles in basic solutions of small tetraalkylammonium cations. *J. Phys. Chem. B* **2004**, *108*, 12271−12275.
(22) Fedeyko, J. M.; Vlachos, D. G.; Lobo, R. F. Formation and structure of self-assembled silica nanoparticles in basic solutions of organic and inorganic cations. *Langmuir* **2005**, *21*, 5197−5206.
(23) Rivas-Cardona, A.; Chovanetz, M.; Shantz, D. F. A systematic investigation of silicalite-1 precursor mixtures with varying degrees of dilution. *Microporous Mesoporous Mater.* **2012**, *155*, 56−64.
(24) Kumar, S.; Wang, Z.; Penn, R. L.; Tsapatsis, M. A structural resolution cryo-TEM study of the early stages of MFI growth. *J. Am. Chem. Soc.* **2008**, *130*, 17284−17286.
(25) Kumar, S.; Penn, R. L.; Tsapatsis, M. On the nucleation and crystallization of silicalite-1 from a dilute clear sol. *Microporous Mesoporous Mater.* **2011**, *144*, 74−81.
(26) Lesthaeghe, D.; Vansteenkiste, P.; Verstraelen, T.; Ghysels, A.; Kirschhock, C. E. A.; Martens, J. A.; Speybroeck, V. V.; Waroquier, M. MFI fingerprint: How pentasil-induced IR bands shift during zeolite nanogrowth. *J. Phys. Chem. C* **2008**, *112*, 9186−9191.
(27) Aerts, A.; Haouas, M.; Caremans, T. P.; Follens, L. R. A.; van Erp, T. S.; Taulelle, F.; Vermant, J.; Martens, J. A.; Kirschhock, C. E. A. Investigation of the mechanism of colloidal silicalite-1 crystallization by using DLS, SAXS, and ^{29}Si NMR spectroscopy. *Chem.—Eur. J.* **2010**, *16*, 2764−2774.
(28) Lupulescu, A. I.; Rimer, J. D. In situ imaging of silicalite-1 surface growth reveals the mechanism of crystallization. *Science* **2014**, *344*, 729−732.
(29) Mora-Fonz, M. J.; Catlow, C. R. A.; Lewis, D. W. Oligomerization and cyclization processes in the nucleation of microporous silicas. *Angew. Chem., Int. Ed.* **2005**, *117*, 3142−3146.
(30) Mora-Fonz, M. J.; Catlow, C. R. A.; Lewis, D. W. Modeling aqueous silica chemistry in alkali media. *J. Phys.Chem. C* **2007**, *111*, 18155−18158.
(31) Auerbach, S. M.; Fan, W.; Monson, P. A. Modelling the assembly of nanoporous silica materials. *Int. Rev. Phys. Chem.* **2015**, *34*, 35−70.

DOI: 10.1021/acs.langmuir.5b00382
Langmuir 2015, 31, 4940−4949

(32) Rankin, S. E.; Kasehagen, L. J.; McCormick, A. V.; Macosko, C. W. Dynamic Monte Carlo simulation of gelation with extensive cyclization. *Macromolecules* **2000**, *33*, 7639−7648.
(33) Wu, M. G.; Deem, M. W. Monte Carlo study of the nucleation process during zeolite synthesis. *J. Chem. Phys.* **2002**, *116*, 2125−2137.
(34) Rao, N. Z.; Gelb, L. D. Molecular dynamics simulations of the polymerization of aqueous silicic acid and analysis of the effects of concentration on silica polymorph distributions, growth mechanisms, and reaction kinetics. *J. Phys. Chem. B* **2004**, *108*, 12418−12428.
(35) Zhang, X.-Q.; Trinh, T. T.; van Santen, R. A.; Jansen, A. P. J. Structure-directing role of counterions in the initial stage of zeolite synthesis. *J. Phys. Chem. C* **2011**, *115*, 9561−9567.
(36) Zhang, X.-Q.; Trinh, T. T.; van Santen, R. A.; Jansen, A. P. J. Mechanism of the initial stage of silicate oligomerization. *J. Am. Chem. Soc.* **2011**, *133*, 6613−6625.
(37) Zhang, X.-Q.; van Santen, R. A.; Jansen, A. P. J. Kinetic Monte Carlo modeling of silicate oligomerization and early gelation. *Phys. Chem. Chem. Phys.* **2012**, *14*, 11969−11973.
(38) Jorge, M.; Auerbach, S. M.; Monson, P. Modeling spontaneous formation of precursor nanoparticles in clear-solution zeolite synthesis. *J. Am. Chem. Soc.* **2005**, *127*, 14388−14400.
(39) Jin, L.; Auerbach, S. M.; Monson, P. A. Modeling nanoparticle formation during early stages of zeolite growth: A low-coordination lattice model of template penetration. *J. Phys. Chem. C* **2010**, *114*, 14393−14401.
(40) Malani, A.; Auerbach, S. M.; Monson, P. A. Probing the mechanism of silica polymerization at ambient temperatures using Monte Carlo simulations. *J. Phys. Chem. Lett.* **2010**, *1*, 3219−3224.
(41) Malani, A.; Auerbach, S. M.; Monson, P. A. Monte Carlo simulations of silica polymerization and network formation. *J. Phys. Chem. C* **2011**, *115*, 15988−16000.
(42) Devreux, F.; Boilot, J. P.; Chaput, F.; Lecomte, A. Sol-gel condensation of rapidly hydrolyzed silicon alkoxides: A joint ^{29}Si NMR and small-angle x-ray scattering study. *Phys. Rev. A* **1990**, *41*, 6901−6909.
(43) Hammonds, K. D.; Heine, V.; Dove, M. T. Rigid-unit modes and the quantitative determination of the flexibility possessed by zeolite frameworks. *J. Phys. Chem. B* **1998**, *102*, 1759−1767.
(44) Astala, R.; Auerbach, S. M.; Monson, P. A. Normal mode approach for predicting the mechanical properties of solids from first principles: Application to compressibility and thermal expansion of zeolites. *Phys. Rev. B* **2005**, *71*, 014112.
(45) Astala, R.; Auerbach, S. M.; Monson, P. A. Density functional theory study of silica zeolite structures: stabilities and mechanical properties of SOD, LTA, CHA, MOR, and MFI. *J. Phys. Chem. B* **2004**, *108*, 9208−9215.
(46) Jin, L.; Auerbach, S. M.; Monson, P. A. Simulating the formation of surfactant-templated mesoporous silica materials: a model with both surfactant self-assembly and silica polymerization. *Langmuir* **2013**, *29*, 766−780.
(47) Dupree, E.; Pettifer, R. F. Determination of the Si-O-Si bond angle distribution in vitreous silica by magic angle spinning NMR. *Nature* **1984**, *308*, 523−525.
(48) Keskar, N. R.; Chelikowsky, J. R. Structural properties of nine silica polymorphs. *Phys. Rev. B* **1992**, *46*, 1−13.
(49) Pereira, J. C. G.; Catlow, C. R. A.; Price, G. D. Molecular dynamics simulation of methanolic and ethanolic silica-based sol-gel solutions at ambient temperature and pressure. *J. Phys. Chem. A* **2002**, *106*, 130−148.
(50) Stillinger, F. H.; Weber, T. A. Computer simulation of local order in condensed phases of silicon. *Phys. Rev. B* **1985**, *31*, 5262−5271.
(51) Molinero, V.; Moore, E. B. Water modeled as an intermediate element between carbon and silicon. *J. Phys. Chem. B* **2009**, *113*, 4008−4016.
(52) Caratzoulas, S.; Vlachos, D. G.; Tsapatsis, M. Potential of mean force for tetramethylammonium binding to cagelike oligosilicates in aqueous solution. *J. Am. Chem. Soc.* **2006**, *128*, 16138−16147.
(53) Johnson, J. K.; Panagiotopoulos, A. Z.; Gubbins, K. E. Reactive canonical Monte Carlo A new simulation technique for reacting or associating fluids. *Mol. Phys.* **1994**, *81*, 717−733.
(54) Smith, W. R.; Triska, B. The reaction ensemble method for the computer simulation of chemical and phase equilibria. I. Theory and basic examples. *J. Chem. Phys.* **1994**, *100*, 3019−3027.
(55) Richard, A.; Catlow, C.; Ackermann, L.; G. Bell, R.; Cora, F.; H. Gay, C.-D.; A. Nygren, M.; Carlos Pereira, J.; Sastre, G.; Slater, C.-B.; E. Sinclair, P. Introductory lecture computer modelling as a technique in solid state chemistry. *Faraday Discuss.* **1997**, *106*, 1−40.
(56) Rimer, J. D.; Lobo, R. F.; Vlachos, D. G. Physical basis for the formation and stability of silica nanoparticles in basic solutions of monovalent cations. *Langmuir* **2005**, *21*, 8960−8971.
(57) Ravishankar, R.; Kirschhock, C. E. A.; Knops-Gerrits, P.-P.; Feijen, E. J. P.; Grobet, P. J.; Vanoppen, P.; de Schryver, F. C.; Miehe, G.; Fuess, H.; Schoeman, B. J.; Jacobs, P. A.; Martens, J. A. Characterization of nanosized material extracted from clear suspensions for MFI zeolite synthesis. *J. Phys. Chem. B* **1999**, *103*, 4960−4964.
(58) Kragten, D. D.; Fedeyko, J. M.; Sawant, K. R.; Rimer, J. D.; Vlachos, D. G.; Lobo, R. F.; Tsapatsis, M. Structure of the silica phase extracted from Silica/(TPA)OH solutions containing nanoparticles. *J. Phys. Chem. B* **2003**, *107*, 10006−10016.
(59) Yuan, X.; Cormack, A. Efficient algorithm for primitive ring statistics in topological networks. *Comput. Mater. Sci.* **2002**, *24*, 343−360.
(60) Knops-Gerrits, P.-P.; Vos, D. E. D.; Feijen, E. J.; Jacobs, P. A. Raman spectroscopy on zeolites. *Microporous Mater.* **1997**, *8*, 3−17.

DOI: 10.1021/acs.langmuir.5b00382
Langmuir 2015, 31, 4940−4949